

# A New Model for the Surface Arrangement of Myosin Molecules in Tarantula Thick Filaments

Gerald Offer<sup>1,2,4\*</sup>, Peter J. Knight<sup>1,3</sup>, Stanley A. Burgess<sup>1,3</sup>  
Lorenzo Alamo<sup>4</sup> and Raúl Padrón<sup>4</sup>

<sup>1</sup>*Division of Molecular and Cellular Biology, Department of Clinical Veterinary Science University of Bristol, Langford Bristol BS40 5DS, UK*

<sup>2</sup>*Department of Physiology Medical School, University of Bristol, University Walk Bristol BS8 1TD, UK*

<sup>3</sup>*School of Biomedical Sciences University of Leeds, Leeds LS2 9JT, UK*

<sup>4</sup>*Department of Structural Biology, Venezuelan Institute for Scientific Research (IVIC) Apdo 21827, Caracas 1020A, Venezuela*

Three-dimensional reconstructions of the negatively stained thick filaments of tarantula muscle with a resolution of 50 Å have previously suggested that the helical tracks of myosin heads are zigzagged, short diagonal ridges being connected by nearly axial links. However, surface views of lower contour levels reveal an additional J-shaped feature approximately the size and shape of a myosin head.

We have modelled the surface array of myosin heads on the filaments using as a building block a model of a two-headed regulated myosin molecule in which the regulatory light chains of the two heads together form a compact head-tail junction. Four parameters defining the radius, orientation and rotation of each myosin molecule were varied. In addition, the heads were allowed independently to bend in a plane perpendicular to the coiled-coil tail at three sites, and to tilt with respect to the tail and to twist at one of these sites. After low-pass filtering, models were aligned with the reconstruction, scored by cross-correlation and refined by simulated annealing.

Comparison of the geometry of the reconstruction and the distance between domains in the myosin molecule narrowed the choice of models to two main classes. A good match to the reconstruction was obtained with a model in which each ridge is formed from the motor domain of a head pointing to the bare zone together with the head-tail junction of a neighbouring molecule. The heads pointing to the Z-disc intermittently occupy the J-position. Each motor domain interacts with the essential and regulatory light chains of the neighbouring heads. A near-radial spoke in the reconstruction connecting the backbone to one end of the ridge can be identified as the start of the coiled-coil tail.

© 2000 Academic Press

*Keywords:* myosin; thick filament; cross-bridges; three-dimensional reconstruction; muscle

\*Corresponding author

## Introduction

The thick filaments of relaxed tarantula muscles are exceptionally well ordered (Wray, 1982; Levine *et al.*, 1983; Crowther *et al.*, 1985; Padrón *et al.*, 1999). In common with the thick filaments of *Limulus* and scorpion which they resemble, they therefore make particularly suitable subjects for determining the configuration of myosin heads on the surface of the filament and the manner in

which the heads of neighbouring molecules interact.

The structure of this class of myosin filaments has been investigated by X-ray diffraction of relaxed muscles (Wray *et al.*, 1974, 1975; Wray, 1982) and by electron microscopy of negatively stained thick filaments (Kensler & Levine, 1982; Kensler *et al.*, 1985; Stewart *et al.*, 1981, 1985; Levine *et al.*, 1983; Crowther *et al.*, 1985), rapidly frozen thick filaments (Padrón *et al.*, 1999) or sections of relaxed muscle (Padrón *et al.*, 1993, 1995). The filaments have four-fold rotational symmetry with four myosin molecules forming a “crown” of cross-bridges at each axial level 145 Å apart. The myosin heads are arranged on a right-handed four-start helical surface lattice with a pitch of

Abbreviations used: RLC, regulatory light chain; ELC, essential light chain; S1, chicken skeletal subfragment-1.

E-mail address of the corresponding author: [g.w.offer@bristol.ac.uk](mailto:g.w.offer@bristol.ac.uk)

$12 \times 145 \text{ \AA}$ . This implies that there is a rotation of  $30^\circ$  between successive crowns and that the structure repeats at  $3 \times 145 \text{ \AA}$  intervals. The distribution of intensity in the X-ray diffraction pattern suggested that the principal diffracting unit was elongated and tilted axially by at least  $30^\circ$  from the normal to the filament axis and slewed by  $\sim 60^\circ$  (Wray *et al.*, 1974, 1975). Three-dimensional reconstructions of electron micrographs (Crowther *et al.*, 1985; Stewart *et al.*, 1985) confirmed this general picture and showed that the helical tracks of heads had a zigzag pattern with the long axis of the heads close to the surface of the backbone. The morphological unit was considered to be a short diagonal ridge together with a nearly axial link connecting that ridge to a neighbouring ridge (Crowther *et al.*, 1985; Stewart *et al.*, 1985). The appearance of the reconstruction was explained if the two heads of a myosin molecule are splayed. It was originally suggested that one head pointed approximately axially towards the bare zone and the other pointed away from the bare zone and was inclined at about  $45^\circ$  to the filament axis. In this interpretation the anti-parallel heads of axially neighbouring molecules overlapped one another only at their tips. However, Levine *et al.* (1988) pointed out that the lattice points of neighbouring molecules along a helical track were separated by  $\sim 16 \text{ nm}$ , approaching the length of the myosin head. Taking into account new evidence that the active sites of interacting heads from adjacent levels were close, they therefore proposed an alternative splayed model in which the heads from neighbouring axial levels nearly completely overlapped one another, one head at a higher radius than the other.

The intermolecular head-head interactions between neighbouring myosin molecules in the relaxed state may contribute to the regulatory mechanism by sequestering the heads away from actin (Crowther *et al.*, 1985; Vibert & Craig, 1985; Craig *et al.*, 1987; Levine *et al.*, 1991; Padrón *et al.*, 1991). On activation of tarantula muscle, phosphorylation of the myosin regulatory light chains (RLCs) (Sellers, 1981) causes the heads to dissociate from one another and become disordered (Craig *et al.*, 1987; Padrón *et al.*, 1991). In view of the possible physiological significance of these intermolecular interactions to myosin-linked regulation and cooperativity (Chantler *et al.*, 1981), it is important to determine their nature.

The determination of the atomic structure of chicken skeletal subfragment-1 (S1), the proteolytically cleaved myosin head (Rayment *et al.*, 1993), has opened the way to modelling of the cross-bridge surface array. Padrón *et al.* (1998) fitted the morphological unit of the three-dimensional reconstruction with two closely packed anti-parallel S1 molecules. Their model resembles that of Levine *et al.* (1988) in having extensive overlap of neighbouring heads with a substantial interface between the motor domains, but the heads are axially, rather than radially, staggered. Such modelling

using only S1 has the advantage that no constraints are placed on the relative orientation of the two heads of the same myosin molecule which are known to adopt a variety of angles with respect to one another (Slayter & Lowey, 1967; Mendelson *et al.*, 1973; Elliott & Offer, 1978). However, because these heads are actually tethered to a coiled-coil tail, there are constraints on the relative disposition of the two heads which modelling with S1 may not reflect. Hence, it is important also to model the thick filament with a two-headed molecule. Such modelling would have the additional advantage that the head-tail junction itself may contribute to features in the reconstruction which might otherwise be unexplained. Recently we obtained a plausible model of the head-tail junction of the myosin molecule by superposing the C-terminal  $\alpha$ -helix of the scallop regulatory domain or chicken S1 on each of the two  $\alpha$ -helical strands of a model of the coiled-coil tail (Offer & Knight, 1996). In this model the two heads contact one another through their RLCs thus accounting for the intramolecular head-head interactions that underlie cooperativity and regulation in the molecule (Szent-Györgyi & Chantler, 1994).

Here, we have endeavoured to explain the reconstruction by using the known helical symmetry of the filament to build models of the surface array of cross-bridges from a two-headed model of a regulated myosin molecule. By comparison of the geometry of the reconstruction with the separation of domains in the myosin molecule, we have been able to restrict the number of possible models that needed to be examined to two main classes. Rather than fitting molecules within a contour of protein density, we have used objective methods to fit the entire protein density distribution of the cross-bridge annulus. We aimed to determine the orientation of the two heads of each myosin molecule in the filament and how each myosin molecule interacts with its neighbours along the helical tracks. We wished to determine whether a plausible model could be constructed which incorporated both intra- and inter-molecular head-head interactions.

## Results

### Description of reconstruction

Although the three-dimensional reconstruction of negatively stained tarantula thick filaments has been described by Crowther *et al.* (1985), new features that affect the interpretation have emerged on re-examination of the original data in new ways. The morphological unit as seen in surface views or contour plots of the reconstruction at high density levels ( $\sim 100$  on a scale from 0 to 255) consists of a short ridge inclined at  $\sim 72^\circ$  to the filament axis together with a nearly axial link that joins the end of one ridge to the next ridge along the helical track (Figures 1(c) and 2(c)). The repetition of these elements produces each of the four

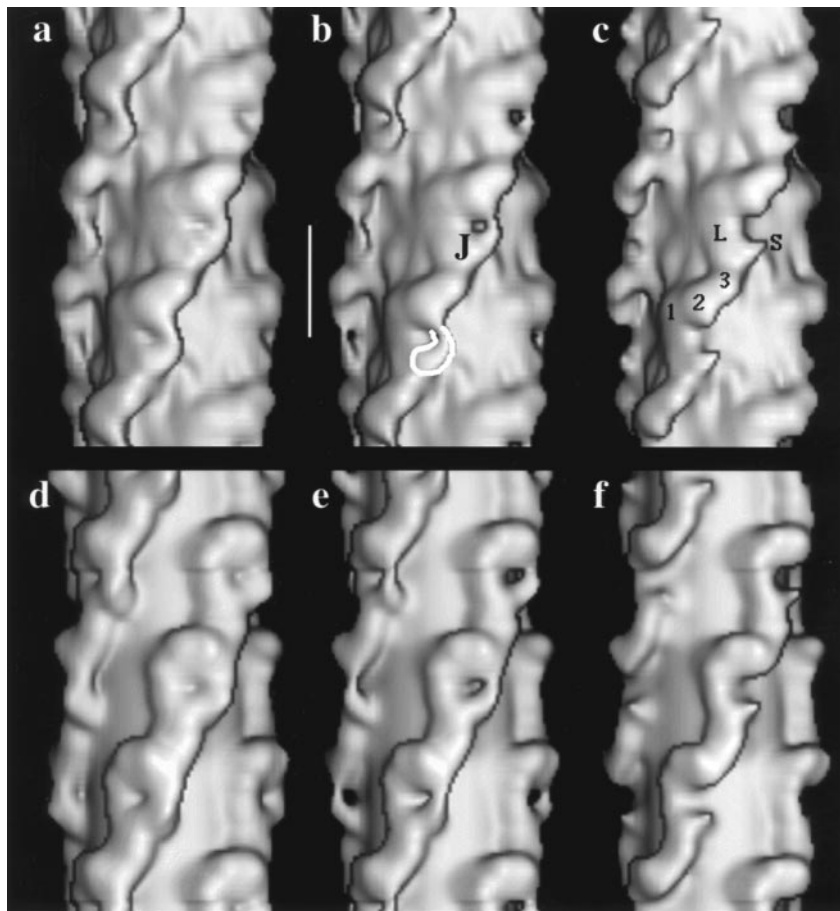


**Figure 1.** Comparison of surface views of the reconstruction and the refined RJ model. The reconstruction at contour levels (a) 60; (b) 80 and (c) 100. The refined RJ model at contour levels (d) 30; (e) 50 and (f) 70. D1, D2 and D3 of the ridge are labelled 1, 2, 3. A link is labelled (L); a J-shaped feature (J) and a spur (S). Another J-shaped feature has been outlined in white. Surface views were obtained with SPIDER. Because of the lower background density in the model than in the reconstruction, lower contour densities were required for the model than for the reconstruction for their appearances to be matched. A scale bar shown in (b) represents 145 Å.

zigzag helical tracks. In transverse slices through the reconstruction, the ridges are seen as four prominent anti-clockwise blades when viewed from the bare zone towards the Z-disc (Figure 3(a), slices 2-3). This gives the filament a propeller-like appearance reminiscent of the configuration of bridges deduced from X-ray diffraction of relaxed *Limulus* muscle (Wray *et al.*, 1975). In slices centred nearer the Z-disc end of a ridge (slice 2), each blade is slewed at an angle of  $\sim 74^\circ$  and is only slightly curved, but nearer the centre of the ridge (slice 3) the blade becomes more curved reflexing back towards the backbone. When the slices are centred on the bare-zone end of the ridge, the blade is replaced by a single peak of density which connects to the backbone with a clockwise curvature (slices 4 and 5). The nearly axial links are seen as four features of high density appearing at a similar azimuthal position (slices 6, 7 and 1).

Each ridge is differentiated into three regions of high density, successively D1, D2 and D3 proceeding along a ridge towards the bare zone (Figures 1(c) and 2). The cylindrical co-ordinates of the peak densities of these features and the distances between them are given in Table 1. Although D1, D2 and D3 are equally spaced azimuthally, the axial separation of D1 and D2 is about half that of D2 and D3 (Figure 2(c)). Consequently the ridge appears slightly bent at its centre

when the filament is viewed side-on. D1 has a radius (108 Å) only a little higher than the backbone, whereas D2 and D3 have a higher radius ( $\sim 128$  Å) causing the ridge to appear as a blade in transverse sections (Figure 3). Near D1 the ridge emerges from the backbone at an acute angle in end-on view but near D3 its connection with the backbone is more nearly perpendicular (Figure 2(a) and (b)). The ridge is clearly separated from the backbone near D2.

Each nearly axial link is  $\sim 78$  Å long measured between the edges of neighbouring ridges at contour level 100. It is slightly curved, and proceeding towards the Z-disc from its connection with D1, it tilts inwards towards the backbone to reach its lowest radius of 93 Å about 25 Å from D1. It then tilts more gradually outwards to connect with D3 in the ridge nearer the Z-disc. It does not connect centrally to D3 but at a lower radius than that of the peak density of D3 (Figure 2(b) and (c)). It has its highest density ( $\sim 230$ ) near its connection with D1, and D1 is resolved from it only at very high contour levels ( $\sim 240$ ).

Within D3, near its contact with the link, there is a connection to the backbone which we call the spoke (Figure 2(b)). We call the origin of the spoke within D3 the spoke junction; its cylindrical coordinates are given in Table 1A. The spoke is tilted at an angle of  $\sim 80^\circ$  to the filament axis. When

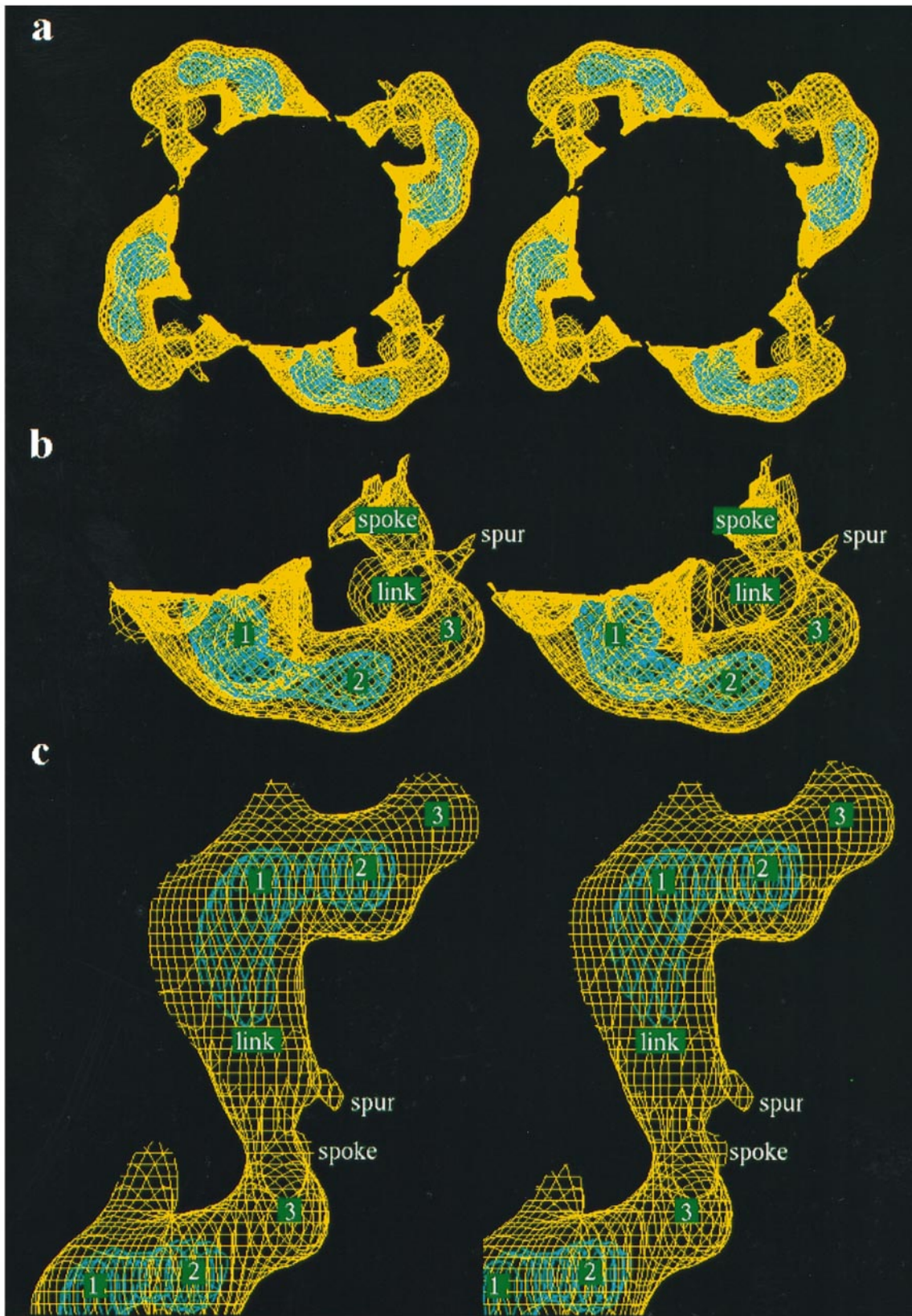


**Figure 2.** Stereo pairs of contour plots of the reconstruction. (a) End-on view of segment 145 Å long. (b) as (a) but at higher magnification and showing only a quarter of the filament. Near the viewer is the link close to its junction with D3 of the ridge. The spoke which connects this junction with the backbone is marked. (c) Side-view of one helical track. D1, D2 and D3 of a ridge are labelled 1, 2 and 3. The contour levels shown are 135 (yellow) and 200 (blue). The low radius features of any helical reconstruction are the least reliable. Moreover, in tarantula filaments the symmetry of the backbone may not be the same as that of the myosin heads since paramyosin is present. Indeed, in the

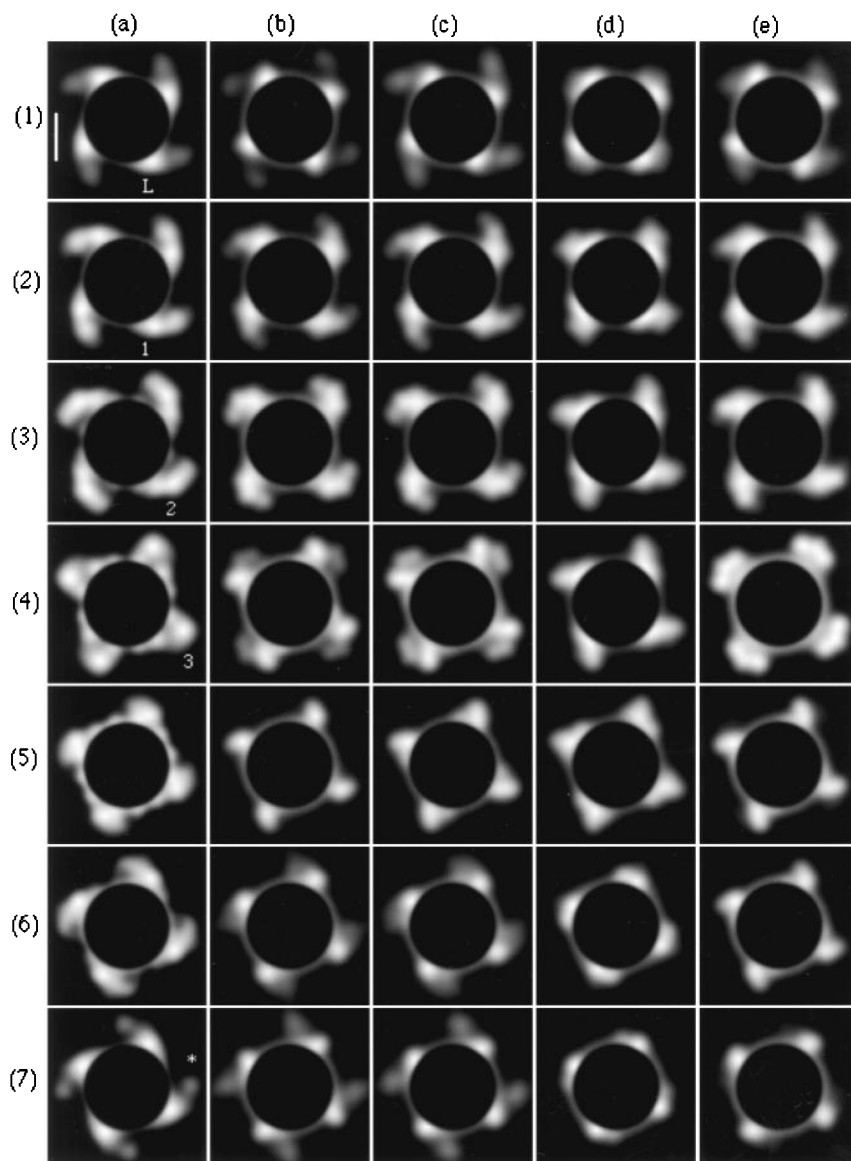


**Figure 3.** Comparison of serial transverse slices of the reconstruction and of filament models. (a) Reconstruction, (b) the RJ model refined by simulated annealing (run d) (c) the RRJ model refined by simulated annealing (run h) (d) the original Padrón *et al.* (1998) model made from S1 (e) the RR model refined by the downhill simplex method (run f). The thickness of the slices is 7.25 Å and the set of seven slices spans an axial interval of 145 Å. The eighth slice would be identical to the first except for a 30° rotation. Each series progresses down a column in a direction towards the bare zone. The view is from the bare zone towards the Z-disc. Models were stacked, low-pass filtered and aligned against the reconstruction. D1, D2 and D3 of a ridge are labelled 1, 2 and 3. A link is labelled L and a J-shaped feature by an asterisk. The density distributions are shown only for radii greater than 80 Å. The scale bar shown in (a) slice (1) represents 100 Å.

viewed down the filament axis, the spoke is slewed at an angle of  $\sim 30^\circ$  where it meets D3. This spoke is of interest because it may represent the first part of the coiled-coil tail connecting the two myosin heads to the backbone (see below).

Because the heads are only incompletely resolved from the backbone, the radius of the backbone is hard to define but measured between blades it is approximately 90–100 Å. This is consistent with a radius of 100 Å measured in the bare zone (Crowther *et al.*, 1985).

### J-shaped feature

The contours of density lie close to one another on the edge of the ridge nearer the bare zone and the inner and outer surfaces of the ridge; the positions of these surfaces are therefore not greatly dependent on the contour level. However, on the edge of the ridge nearer the Z-disc, particularly near D2, and along the right-hand side of the link in Figures 1(c) and 2(c), especially near the midpoint of the link, the density gradient is much shall-

---

backbone of the original negatively stained filaments there were indications of axially oriented rather than helically arranged subfilaments (Craig & Padrón, 1982; Crowther *et al.*, 1985). Features observed in the backbone of the reconstruction may therefore simply reflect the imposition of the cross-bridge helical symmetry used to calculate the map and we do not consider them reliable. No details of the backbone within a radius smaller than 80 Å are therefore shown. The grid side represents 4.2 Å.

**Table 1.** Geometry of principal features of reconstruction

A. Cylindrical coordinates							
	Radius (Å) <sup>a</sup>	Azimuth (deg.) <sup>a</sup>	Axial position (Å)	Peak density			
Ridge							
D1 (peak)	108	0.0	0	250			
D2 (peak)	127	17.8	9	238			
D3 (peak)	129	34.4	30	195			
Spoke junction	113	31.6	46	145			
Link							
Low radius	93	-2.0	-25	230			
Midpoint	107	-0.7	-60	170			
J-shape							
Spur	117	16.4	-68	135			
Axial part	132	29.8		85			
B. Distances (Å) between principal features within the same morphological unit							
	D2 (peak)	Ridge D3 (peak)	Spoke junction	Link Low radius	Link Midpoint	J-shape Spur	
Ridge							
D1 (peak)	42	79	76	30	60	75	
D2 (peak)	-	42	49	61	81	78	
D3 (peak)		-	24	95	116	105	
Spoke junction		-	-	95	122	118	
Link							
Low radius				-	37	59	
Midpoint					-	36	
C. Distances (Å) between features in neighbouring morphological units along a helical track							
	Unit nearer bare zone						
Unit nearer Z-disc	D1 (peak)	Ridge D2 (peak)	Ridge D3 (peak)	Spoke junction	Link Low radius	Link Midpoint	J-shape Spur
Ridge							
D1 (peak)	155	182	216	222	130	101	118
D2 (peak)	139	159	194	203	117	82	91
D3 (peak)	118	128	160	172	98	61	56
Spoke junction	99	114	146	156	76	40	43
Link							
Low radius	180	204	236	243	153	124	136
Midpoint	212	235	267	275	186	155	164
J-shape							
Spur	214	232	262	274	190	155	157

<sup>a</sup> Radial and azimuthal coordinates were measured on transverse sections of the contour plots, and the axial coordinates on side-views. Azimuthal and axial coordinates are expressed relative to the peak density of D1.

lower and the appearance of surface views in this region is markedly sensitive to the contour level chosen.

In the surface view of contour level 100 (Figure 1(c)) a spur of density is present along the right hand side of the link near its midpoint. In contour level 80 (Figure 1(b)) this spur is much enlarged and follows a curved path to connect up to the next ridge nearer the bare zone between D2 and D3. This J-shaped feature is largely unchanged (apart from enlargement) as the contour level is decreased to 60 (Figure 1(a)) or even down to a level (~10) when islands of noise in the background are apparent. In transverse slices (Figure 3(a), slices 7 and 1), the J-shaped feature can be identified as a circular feature (asterisked) on the anticlockwise side of the sectioned link and separated from it by a gap of lower density.

The J-shaped feature has the approximate size and shape of a myosin head and we think it likely that it is caused by the head pointing to the Z-disc (the Z-wards head) occupying this position. We suppose it is of relatively low density because only a fraction of the Z-wards heads occupy this position at any instant of time. The J-shaped feature, together with the link and the ridge it connects with, forms a lozenge-shaped quadrilateral.

### Contour levels defining the filament surface

It would be useful to define a reference contour that approximately coincided with the filament surface, so that a starting model of the filament could be built with the molecules positioned to lie inside it. Contours of density <150 contain the backbone as well as all four helical tracks

(Figure 2(a)). However, the volume of heads enclosed by each contour level can be calculated by assuming that the backbone is cylindrical and subtracting the backbone volume from the total volume enclosed. Based on a molecular weight of 137 kDa per head and a specific volume of 0.74 ml/g, the volume of the eight heads present per 145 Å length of filament is  $1.35 \times 10^6$  Å<sup>3</sup>. For backbone radii in the range 90–100 Å, reference contour levels in the range 94 to 114 enclose this volume. This is consistent with previous modelling (Padrón *et al.*, 1998) when the two S1 molecules were fitted largely within a reference contour of 100. However, this range of contour levels must be considered only as a guide. Firstly, after low-resolution imaging, the proximity of a strong neighbouring feature may distort the position of the contours so no single reference contour will exactly follow the filament surface. Secondly, the concept of a reference contour is straightforward only if both heads are equally represented in the reconstruction and each fully occupies only one position. If, as suggested above, one of the heads is mobile and occupies a position only intermittently, that position will be represented by relatively weak density. Consequently, the reference contour as defined above will lie outside the molecular boundary of the high-occupancy features and inside that of the low-occupancy features (or not even reveal the low occupancy features). For example, suppose the ELC domain and motor domain of one head intermittently occupies the J-shaped feature while the high density features of the reconstruction are formed by the head-tail junction and the motor domain and ELC domain of the other head. The appropriate reference contour level containing the volume for four head-tail junctions, four ELC domains and four motor domains per 145 Å filament lies in the range 124 to 137 for backbone radii 90–100 Å.

### Model of regulated myosin

*Tarantula* myosin is regulated but its structure has not been determined. We therefore based our building block for the thick filament on the scallop structure since scallop myosin is also regulated. We started with a model of the head-tail junction of scallop myosin made as previously described (Offer & Knight, 1996) by joining the crystal structure of a scallop regulatory domain (in the presence of Ca<sup>2+</sup>) to a model of the first 102 residues of the scallop coiled coil-tail i.e. residues up to residue 936 of the scallop heavy chain. To complete the structure of the molecule requires the addition of a motor domain for each head. We used the proposal of Houdusse & Cohen (1996) to position a chicken skeletal motor domain (Rayment *et al.*, 1993) onto the head-tail junction in such a way that the ELC/motor interface resembled that in chicken S1. To decrease the computational load in modelling the filament, only the C<sup>α</sup> atoms were used. The model is shown in Figure 4(a) and (b). As con-

structed, the molecule retains the dyad axis of the coiled coil and in end-on view (Figure 4(b)) the two heads form an S-shape. The curvature of the heads arises from the fact that the head-tail junction, the ELC domain and the motor domain are joined to one another at an angle. Looking down the coiled-coil axis the head-tail junction is diamond-shaped and about 79 Å long by 55 Å wide (Figure 4(b)); in side-view (Figure 4(a)) it is only about 31 Å measured along the coiled coil axis. The proline residues that mark the start of the coiled coil lie at the face of this head-tail junction nearest the coiled coil.

### Bending of heads

The myosin head is capable of bending at several places both spontaneously and as a result of binding different nucleotides (Wakabayashi *et al.*, 1992; Sugimoto *et al.*, 1995; Whittaker *et al.*, 1995; Fisher *et al.*, 1995; Mendelson *et al.*, 1996; Offer & Knight, 1996; Houdusse & Cohen, 1996; Burgess *et al.*, 1997; Dominguez *et al.*, 1998). We therefore allowed both heads independently to torsionally twist at residue 799 of the scallop heavy chain (located between the ELC and RLC domains) by rotation of the distal part of the head about an axis aligned along the long  $\alpha$ -helix (between residue 799 and residue 824) and to tilt towards or away from the tail by rotation of the distal part of the head about an axis normal both to this axis and the coiled coil axis (Figure 4(b)). We also allowed bending of the heads in a plane perpendicular to the coiled coil at residue 799, residue 784 (located between the two domains of the ELC), and residue 770 (in the motor domain at the start of the long  $\alpha$ -helix) (Figure 4(a)).

### Creating thick filament models

For each myosin molecule, four additional parameters need to be defined to place the molecule within the filament: the radius of the head-tail junction from the filament axis, the tilt and slew of the molecule and the rotation about the molecular axis (Figure 5). The radius of the head-tail junction was defined to be the radius of the local origin of each myosin molecule. The orientation of the molecule is defined in part by the tilt angle made by the coiled-coil axis to the filament axis (Figure 5). A tilt angle of 0° would refer to the case where the tail lay parallel to the filament axis with its free end closer to the bare zone. The slew angle, the azimuthal angle that the axis of the start of the coiled coil makes to a radius in end-on view, was defined such that a slew of 0° corresponded to the case where the coiled-coil tail appeared radial when the filament was viewed end-on. The final parameter that needs to be specified is the rotation of the molecule about its coiled-coil axis. Once the orientation and position of one myosin molecule was determined, that of other molecules were

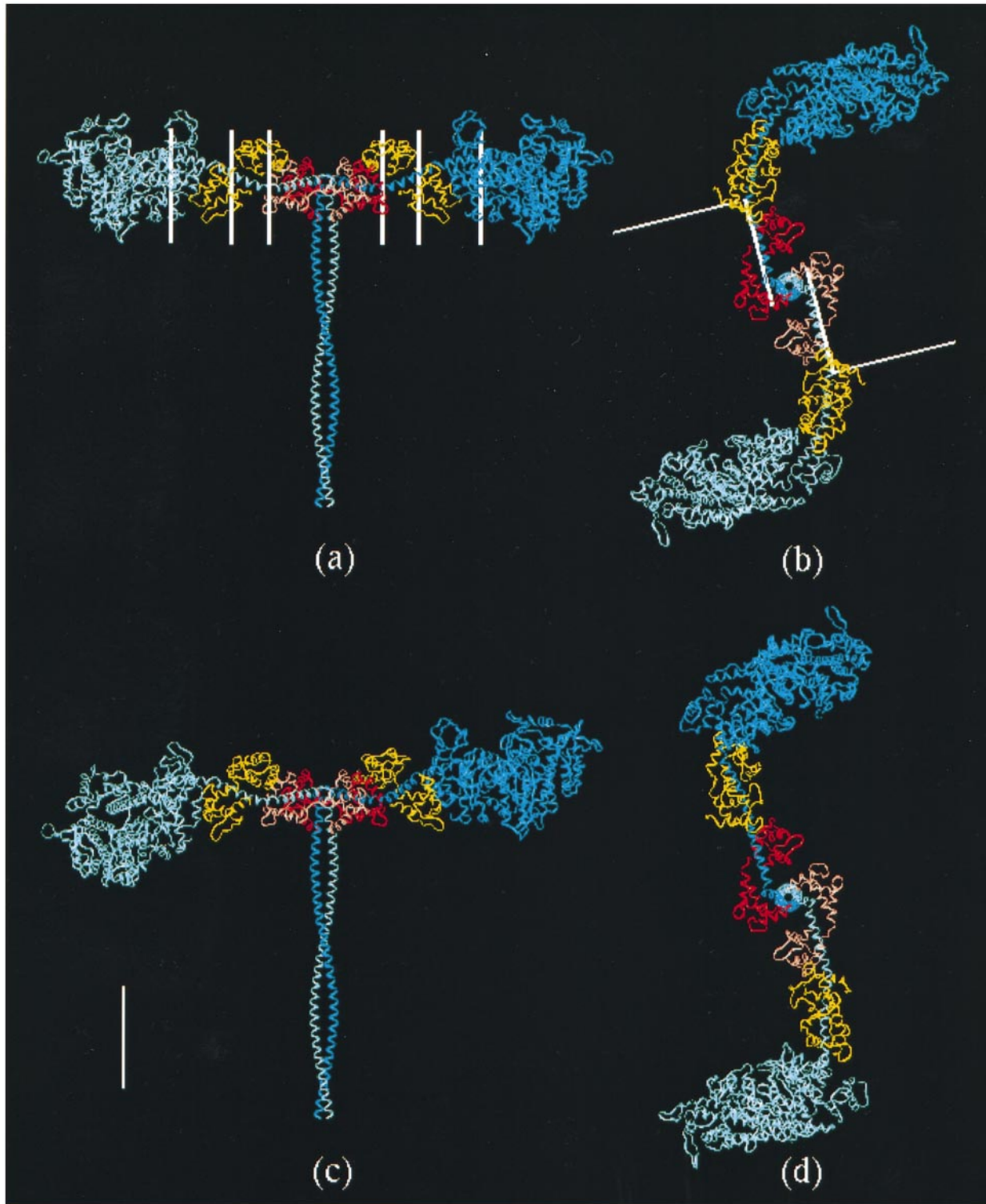


**Figure 4.** Model of a molecule of regulated myosin (a) in side-view (b) in end-on view. (c) and (d) Show corresponding views of the molecule after bending to form the best RJ model. The heavy chains are shown as ribbons in pale blue and mid-blue, the ELC's in yellow and the RLC's in pink and red. (a) Three axes in each head where rotation in a plane perpendicular to the coiled coil tail was allowed. (b) Two axes in each head, rotation about which allowed the heads to tilt towards or away from the tail and to torsionally twist. To construct the filament models the local z-axis of the myosin molecule was defined to be coincident with the coiled-coil axis. The origin and the local x-axis were chosen so that in end-on view the x-axis passed through the  $C^\alpha$  atom of Trp824 of the scallop heavy chain of both heads. In this way the local y-axis lies approximately parallel to the long  $\alpha$ -helices in the regulatory domains of both heads. The scale bar represents 50 Å.

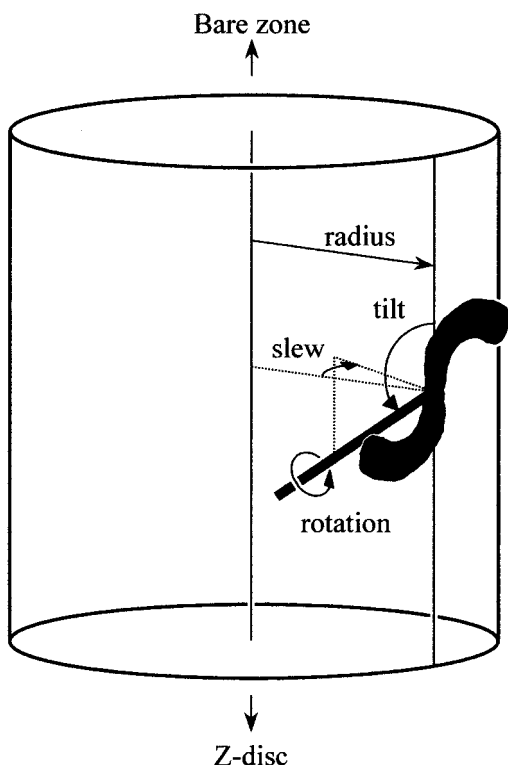


**Figure 5.** The four parameters used to define the position and orientation of myosin molecules in a filament model. Slew is considered positive if, viewed along the filament axis towards the Z-disc, the start of the coiled-coil tail is rotated clockwise compared with a position in which it pointed radially towards the filament axis. In creating the models, the coiled-coil tail was retained only up to residue 863 of the scallop heavy chain (i.e. a total of only 29 residues in each strand).

generated by the known helical symmetry of the filament.

### Inferences from the reconstruction about the disposition of myosin heads

Analysis of the reconstruction helps to define how the myosin molecules pack to form the morphological unit and to reduce the number of classes of model to be considered. The high density of D1, D2 and D3 of the ridge, and one end of the nearly axial link, suggests that they arise from prominent features of the myosin molecule. The relative strength of the features in the reconstruction should reflect the relative masses of the myosin domains that form them. The motor domains ( $\sim 75$  kDa, Rayment *et al.*, 1993) should give rise to prominent features in the reconstruction. Because the motor domain is roughly twice as long as wide, we treated it as having proximal and distal halves. The ELCs with their associated heavy chain (ELC domains) have a mass of  $\sim 30$  kDa and should therefore give rise to a smaller feature. The RLCs of tarantula myosin have a higher molecular weight ( $\sim 26$  kDa) than in other regulated myosins

(Craig *et al.*, 1987). In our model of the head-tail junction, the RLCs of the two heads lie in close proximity and form with the start of the coiled coil a compact globular region (Offer & Knight, 1996). The tarantula head-tail junction thus has a mass of  $\sim 62$  kDa and might give rise to a feature nearly as prominent as that of a motor domain.

The interpretation of the reconstruction is aided by comparing the size of the ridges with that of the motor domain. Measured at a contour level of 100, the ridge is about  $137$  Å long (Figure 2(b) and (c)). This compares with the length ( $\sim 90$  Å) of a motor domain (Rayment *et al.*, 1993). So a motor domain is too short to span the entire length of a ridge but could span the length of either D1 + D2 or D2 + D3. The remainder of the length of the ridge could be formed from an ELC domain or a head-tail junction or from an overlapping motor domain.

To compare the widths of the ridge and a myosin head they must be viewed from similar directions. In order to explain the narrow annulus in which the myosin heads lie, the tilt of our myosin molecule needs to be approximately normal to the filament axis so that the S-shape of the two heads is close to the filament surface. Viewed along the filament axis (Figure 2(b)), the ridge is  $\sim 48$  Å wide at D2. Correspondingly, viewing our regulated myosin molecule normal to its axis (Figure 4(a)), the motor domain is  $\sim 53$  Å and  $\sim 61$  Å wide in the proximal and distal parts. Hence, the ridge is wide enough to accommodate only one head in a radial direction. Models in which the heads are radially staggered (Levine *et al.*, 1988) would therefore not fit the reconstruction.

Viewed side-on (Figure 2(c)), the ridge is  $60$  Å wide at D2 but only  $43$  Å wide at D3. Correspondingly, viewing our regulated myosin molecule down its axis (Figure 4(b)), a motor domain appears uniformly  $\sim 46$  Å wide. The ridge is thus more than wide enough in an axial direction at the position of D2 to accommodate one motor domain but not wide enough to accommodate two axially staggered motor domains. Two explanations are possible. The first is that the ridge might be occupied by only one head and hence the reference contour level defining the ridge should have a higher value ( $\sim 130$ ). The length of the ridge defined by this higher contour level is  $126$  Å, and its width in side-on view is  $\sim 44$  Å at D1,  $\sim 47$  Å at D2 and  $\sim 40$  Å at D3. These dimensions are compatible with a single head occupying the ridge. The second explanation is that the Z-wards head occupies the ridge only intermittently. This would be consistent with the shallower gradient on the Z-wards side of the ridge.

### Location of head-tail junction

To reduce the number of models that needed to be examined, it was especially valuable to consider what feature in the reconstruction could be the site of the head-tail junction. As well as being a moder-

ately strong feature, the head-tail junction should connect with the backbone. A further important test is that it should be possible to trace the path of each head in the reconstruction. Thus there should be a pair of features  $\sim 59$  Å from the head-tail junction where the ELC domains of the same molecule are located, features  $\sim 39$  Å from the ELC domains where the proximal motor domains are located, and features  $\sim 40$  Å from the proximal motor domains where the distal motor domains are located (Table 2). Bending within a head, if it occurred by flexing between domains, would not greatly change these spacings.

D1 is at a low radius and merges with the backbone. If D1 were the site of the head-tail junction, the head nearer the Z-disc of each molecule (the Z-wards head) could follow the path of the link, with the distal motor domain on D3 of the previous ridge since this is at a suitable distance (Table 1C). However, the gradient of density along the link is the inverse of what would be expected. Moreover, there is no strong feature at a suitable distance from D1 to be the site of the distal motor domain of the head nearer the bare zone (the B-wards head). Therefore D1 could not be the site of the head-tail junction. D2 is clearly separated from the backbone and therefore can also be ruled out.

D3 of the ridge was a more promising candidate site for the head-tail junction. It has a moderate density, less than that of D1 and D2. With the head-tail junction centred on the peak density of D3, the ELC domain of the B-wards head could be centred at the midpoint of the link (Table 1C). The proximal motor domain of the B-wards head could then be located in the link near the site where it has minimum radius, and the distal motor domain between D1 and D2. The Z-wards head could follow the J-shape since the spur of the same morphological unit is located at a suitable distance

(105 Å) from D3. Such a model with the head-tail junction located on D3 could thus broadly explain both the zigzag and the J-shape of the reconstruction. However, with the head-tail junction centred on the peak density of D3, the B-wards head would be too short for the distal motor domain to be centred on D2 of the next ridge and the position and size of D2 would be unexplained. An attractive variation is that the head-tail junction of a myosin molecule lies at the spoke junction i.e. about 16 Å nearer to the bare zone than the peak density of D3. This would allow the spoke to be the start of the coiled-coil tail. In this case the ELC domain of the B-wards head could again be located in the link but  $\sim 16$  Å nearer the bare zone than the midpoint. The proximal motor domain of the B-wards head could then be centred on D1 and the distal motor domain on D2. The spur of the same morphological unit is 118 Å from the spoke junction (Table 1B) so the Z-wards head could follow the J-shape. We call this the RJ class of model to indicate that one head forms the ridge and the other head the J-shaped feature. In this class each myosin molecule spans between the spur of one morphological unit and D2 of the next unit, a distance of 232 Å. This is similar to the distance of 219 Å between distal motor domains in our regulated myosin molecule as initially constructed (Table 2) indicating that one or both heads would have to straighten only slightly in order to accommodate to this span.

Alternatives to the RJ class arise if the head-tail junction is instead located in the link and we considered several possible sites. Only one appeared promising. If the head-tail junction is located at the midpoint of the link, there is a good correspondence between the locations of the myosin domains and features in the reconstruction. D1 of the same morphological unit is at a suitable distance (60 Å) to be the site of the ELC domain of

**Table 2.** Distances (Å) between domains in model of regulated myosin molecule

	Head 1				Head-tail junction	Head 2			
	Distal motor	Motor	Proximal motor	ELC		ELC	Proximal motor	Motor	Distal motor
Head 1									
Distal motor	-	16	40	76	110	158	194	208	219
Motor		-	23	61	99	151	185	198	208
Proximal motor			-	39	88	143	174	185	194
ELC				-	59	117	143	151	158
Head-tail junction					-	59	88	99	110
Head 2									
ELC						-	39	61	76
Proximal motor							-	23	40
Motor								-	16
Distal motor									-

The distance between two domains is calculated between their centres of mass. The motor domain is defined as the heavy chain from residues 4 to 777 (chicken sequence, Rayment *et al.* 1993). The proximal region of the motor domain is defined as residues 4 to 170, 489 to 518 and 668 to 777 of the heavy chain (chicken sequence). The distal region of the motor domain is defined as residues 171 to 488 and 519 to 667 of the heavy chain (chicken sequence). The ELC domain is defined as the ELC together with residues 778 to 806 of the heavy chain (scallop sequence). The head-tail junction includes both RLCs and heavy chain residues 807 to 841 (scallop sequence).

the B-wards head. D2 is at a suitable distance (42 Å) from D1 to be the site of the proximal motor domain and D3 suitably spaced from D2 (42 Å) to be the site of the distal motor domain of this head. For the Z-wards head, D3 of the previous morphological unit is at a suitable distance to be the site of the ELC domain. Then D2 of that unit is suitably positioned to be the site of the proximal motor domain and D1 that of the distal motor domain. In this class of model the ridge is formed by the overlap of the B-wards and Z-wards heads and we therefore refer to it as an RR model. The arrangement of domains is similar to that in the model proposed by Padrón *et al.* (1998). In this class of model the myosin molecule has to span between D1 of one morphological unit and D3 of the next, a distance of 216 Å. This is very similar to the distance between distal motor domains in our model of regulated myosin, so little change in the S-shape would be required. However, this class of model does not explain the J-shaped feature since the Z-wards head would not be able to reach the spur of the previous morphological unit which is at a distance of 155 Å.

Two other classes of model that have been proposed previously could be eliminated. In the Crowther *et al.* (1985) model the heads were assumed to be straight. The B-wards head was nearly axial with its tip at D1 and thus accounted for D1 and the link. The Z-wards head was inclined at an angle of  $\sim 45^\circ$  to the filament axis and passed through D3 with the distal region of the motor domain on D2; this head thus accounted for D2 and D3. Myosin heads from adjacent axial levels thus interacted through their tips. However, for the B-wards head to be nearly axial, the head-tail junction would need to be located near D3 so that it could reach D1 of the next ridge, but if that were so, the Z-wards head would be too long to terminate at D2 of the same ridge. We conclude that a myosin molecule where the two heads attach to a fully formed coiled coil cannot produce a structure like that proposed by Crowther *et al.* We also considered models in which the two heads of one molecule are parallel, as has been proposed for fish muscle by Hudson *et al.* (1997). For this class of model the two heads would have to lie along the link since the ridges are too short for the heads to lie along this direction. This would be possible for one head if the head-tail junction were located on D3; the distal motor domain of this head could finish on D1 of the next ridge. The distal motor domain of the other head would have to be located on D2 in order to explain the presence of this feature. The distance between D3 and D2 of the next ridge is 128 Å (Table 1C) so this second head would have to be nearly straight, yet there are no indications from the reconstruction of a direct path between these features.

We conclude that the only plausible sites for the head-tail junction are D3 or near the midpoint of the link. We describe below the results of detailed modelling these two possibilities.

## RJ models

In this class of model D3 is the location of the head-tail junction and D1 and D2 arise from a single motor domain, that of the B-wards head. The link is largely formed from the ELC domain of the B-wards head. The J-shaped feature is formed from the ELC domain and motor domain of the Z-wards head. We suggest it is relatively weak because the Z-wards head is mobile and spends only a fraction of its time in this position.

An initial model of this type was produced by manual fitting of the regulated myosin molecule to the contours of the reconstruction. A near-normal tilt angle allowed the two heads to fall into the narrow annulus of the helical tracks. A small positive slew is required to allow the motor domain of the B-wards head to follow the line of D1 and D2. With the head-tail junction centred on D3 the long  $\alpha$ -helix has to be as long as possible to allow the proximal motor domain to reach D1. This requires straightening of the long  $\alpha$ -helix of our regulatory myosin molecule at the RLC/ELC junction and within the ELC domain and an increase in bending at the start of the long  $\alpha$ -helix. Changes in the radius, tilt, slew, rotation of the molecules, the independent bending at three sites along each head, and the torsional twisting and tilting of the heads were made by trial and error until, with the head-tail junction centred on D3, the ELC domain of the B-wards head was positioned near the midpoint of the link and the motor domain positioned along D1 and D2 of the ridge. The ELC domain and motor domain of the Z-wards head were fitted to the J-shaped feature defined by contour level 70.

The model was refined by the downhill simplex method allowing the above parameters to be variables. In addition the weighting of the ELC domain and motor domain of the Z-wards head, and the backbone radius were treated as variables. The spur in the reconstruction has a maximum density of about half that of D1 or D2. We therefore chose a starting value of 0.5 for the occupancy of the Z-wards head. After low-pass filtering to low resolution (50 Å) and alignment with the reconstruction, the models were scored by cross-correlation. As a result of refinement of the starting model by the downhill simplex method, the cross-correlation coefficient increased from 0.897 to 0.947 and the occupancy of the Z-wards head fell to 0.46 (run a in Table 3).

The downhill simplex method is capable only of finding the local best fit rather than the global best fit. Hudson *et al.* (1997) and de Silva (1998) successfully tackled this problem by using simulated annealing to refine their myosin filament models against the X-ray diffraction patterns of relaxed fish and frog skeletal muscle. When we used simulated annealing to refine our starting RJ model, the cross-correlation coefficient rose from 0.897 to 0.952 and the occupancy of the Z-wards head fell to 0.35 (run b in Table 3). Other simulated annealing runs (obtained with different sets of random

**Table 3.** Parameters of tarantula filament models built from two-headed myosin molecules before and after refinement

<b>RJ model</b>																
Starting	0.897	135	100	28	40	B Z	(1) 0.5	-8 -16	60 50	26 30	-40 -45	0 0	100	82.0 97.9	149.5 172.1	116.4 133.0
Downhill simplex (run a)	0.947	129.4	100.5	40.7	35.1	{ B Z	(1) 0.46	2.0 -17.3	69.1 41.1	31.2 30.2	-37.3 -35.3	-29.4 -1.4	97.5	73.6 80.2	142.4 156.4	111.0 118.6
Simulated annealing (run b)	0.952	124.6	113.5	30.9	50.2	{ B Z	(1) 0.35	19.7 -13.9	49.3 4.6	24.0 51.9	-47.9 -49.9	5.2 28.5	97.0	78.0 84.4	159.4 166.2	110.9 125.8
Second starting	0.908	125	90	25	55	B Z	(1) 0.35	-20 10	30 20	20 30	-35 -25	0 10	97	80.4 91.7	152.1 159.1	112.2 123.6
Simulated annealing (run c)	0.950	124.0	105.3	28.4	50.6	{ B Z	(1) 0.32	7.4 2.1	39.2 28.4	23.7 12.3	-43.1 -32.5	-6.3 38.5	98.6	82.2 84.2	161.7 165.2	112.9 124.6
Simulated annealing (run d)	0.951	123.6	104.3	33.9	60.6	{ B Z	(1) 0.37	0.9 5.0	26.6 8.8	9.7 22.3	-24 -32.1	-9.4 22.7	97.3	77.0 83.8	161.7 163.9	111.4 124.8
Simulated annealing (run e)	0.950	125.3	108.8	23.8	51.6	{ B Z	(1) 0.38	0.8 -4.2	19.3 20.0	47.9 19.6	-51.7 -28.3	-19.8 39.1	98.6	77.2 84.9	161.2 165.9	112.0 126.2
<b>RR model</b>																
Starting	0.878	104.7	85.0	29.0	79.7	B Z	(1) 1.0	-22.3 47.9	-23.2 8.5	14.8 -8.6	7.7 -2.5	23.3 10.9	100.0	66.7 79.4	134.2 145.0	92.3 110.8
Downhill simplex (run f)	0.930	119.7	85.7	42.1	78.1	{ B Z	(1) 0.30	-5.9 47.9	-18.6 7.7	14.2 0.0	1.1 -13.4	23.2 7.1	99.8	86.0 90.2	161.5 162.9	112.3 126.1
<b>RRJ model</b>																
Starting	0.893	119.7	85.7	42.1	78.1	{ B Z <sub>1</sub> Z <sub>2</sub>	(1) 0.30 0.70	-5.9 47.9 37	-18.6 7.7 3	14.2 0.0 28	1.1 -13.4 -10	23.2 7.1 3	99.8	86.0 90.2 100.3	161.5 162.9 168.8	112.3 126.1 133.6
Simulated annealing (run g)	0.944	120.4	90.2	40.9	76.9	{ B Z <sub>1</sub> Z <sub>2</sub>	(1) 0.28 0.24	-8.2 51.1 33.4	-17.4 8.7 -6.9	23.3 1.9 31.1	-0.2 -0.6 -9.9	14.7 21.3 2.2	98.3	83.7 84.3 95.4	158.5 159.6 166.8	111.5 122.2 131.0
Simulated annealing (run h)	0.951	118.3	90.7	53.8	75.6	{ B Z <sub>1</sub> Z <sub>2</sub>	(1) 0.23 0.30	-1.3 46.6 28.6	-3.6 8.3 -6.6	14.8 -7.8 29.7	-8.4 4.5 -2.0	17.7 9.9 0.6	96.8	78.3 84.8 93.3	161.0 160.2 164.1	109.3 122.6 129.3
Simulated annealing (run i)	0.949	114.7	87.0	50.7	72.6	{ B Z <sub>1</sub> Z <sub>2</sub>	(1) 0.32 0.29	-9.5 49.4 20.1	-15.7 22.9 5.2	32.8 -2.8 29.5	-21.8 -3.7 -3.7	19.1 20.9 -3.0	95.8	76.2 82.1 96.4	164.1 155.9 163.0	109.5 118.5 129.9
Simulated annealing (run j)	0.950	116.7	86.5	53.1	73.8	{ B Z <sub>1</sub> Z <sub>2</sub>	(1) 0.26 0.26	2.5 44.7 30.6	-10.1 5.2 -0.2	23.6 11.3 36.6	-14.4 -15.7 -9.4	24.2 2.6 -0.6	98.2	84.0 83.8 96.5	163.7 160.4 165.3	111.4 122.0 130.3

For the RRJ models, Z<sub>1</sub> refers to the ridge position and Z<sub>2</sub> to the J-position of the Z-wards head. Values in brackets were fixed. For the bending parameters, a positive value implies straightening of the heads, a negative value implies increased curvature.

numbers) followed different trajectories and gave slightly lower final cross-correlation coefficients.

Changes in the precise positioning of the head-tail junction and ELC domains occurred as a result of this refinement by simulated annealing. The ELC domain of the B-wards head was no longer centred on the midpoint of the link but formed the two-thirds of the link nearest the bare-zone, the remainder of the link being formed from the bare-zone side of the head-tail junction. This explains the taper of the link towards the Z-disc (Figure 2(c)) and the link having its lowest density near its connection with D3. Correspondingly, the head-tail junction was no longer centred on the peak density of D3 but had moved slightly towards the bare zone so that the proline residues commencing the coiled coil were close to the spoke junction. This strongly suggested that the spoke junction is the site where the coiled-coil tail joins the heads.

A second round of modelling was then commenced building on the lessons learned from the first round. To make the second starting structure we now positioned the proline residues commencing the coiled coil at the spoke junction. To fit the B-wards head it was then not necessary to straighten the long  $\alpha$ -helix so much at the RLC/ELC interface or to bend the head so much at the start of the long  $\alpha$ -helix. The cross-correlation coefficient of this second starting structure was 0.908. In three simulated annealing refinements of this structure the cross-correlation coefficient rose to  $\sim 0.95$  (runs c-e in Table 3), similar to that in the first round. The occupancy of the Z-wards head in these refined models was 0.32-0.38. The radial positions of the heads (Table 3) indicated that the heads lay largely outside the backbone, the centres of mass of the B-wards and Z-wards heads having radii similar to those of the ridge. Although the refined models were similar they were not identical. Some of their defining parameters (e.g. radius, pitch, tilt) were similar, whereas others were not. We selected the refined structure from run d as the best, partly because of its high cross-correlation coefficient and partly because the bending angles required from our regulatory myosin molecule were smaller than for the other runs (Table 3, Figure 4(c) and (d)).

Figure 6 shows this best RJ model in side view. Since the tilt is nearly normal to the filament axis, the myosin molecules are seen nearly end on and are therefore S-shaped. The interacting heads form chains of interlocking S-shapes helically winding around the filament axis. The overlapping ends of neighbouring S-shapes along a helical track produce the lozenge-shaped morphological units seen in the reconstruction. The motor domain of the B-wards head of one myosin molecule lies approximately anti-parallel to the motor domain of the Z-wards head of the neighbouring myosin molecule nearer the bare zone along the same helical track. These motor domains are not however in contact; there is a gap of  $\sim 14$  Å between their side chains. The two heads of a myosin molecule contact both the RLC and ELC domains of flanking

myosin molecules along the same helical track (Figure 6). The tip of each head thus lies close to the RLC/ELC interface. Steric clashes were relatively small and confined to those near the tip of the Z-wards head and the light chains of the flanking myosin molecule nearer the Z-disc.

Comparing this best model with the reconstruction (Figure 7), the motor domain of the B-wards head together with the major part of the head-tail junction formed the ridge. The proximal region of the motor domain was located on D1 and the distal region on D2. In side-view the B-wards head was axially too narrow to fill contour level 100, but it fitted contour level 130 well. In transverse sections through the contour plot the B-wards head fitted the ridges well, and there were few residues in the gap between ridge and backbone. The ELC domain of the Z-wards head contributed to the Z-wards side of D2 and D3.

As would be expected from its high cross-correlation coefficient, this best RJ model explains many of the features of the transverse slices of the reconstruction. In Figure 3(b) slices 2 and 3 the motor domain of the B-wards head is sectioned and the filament has a shape resembling a propeller with four anti-clockwise blades. The blades are slewed and, as in the reconstruction, the blades in slice 3 are more curved than those in slice 2. Each blade is not however so sharply differentiated into two peaks of protein density and is narrower at its tip than in the reconstruction. Nearer the bare-zone, slice 4 includes, as well as the tip of the B-wards motor domain, the head-tail junction of the neighbouring molecule, accounting for the appearance of D3 in the reconstruction. The connection to the backbone is in the clockwise sense, just as in the reconstruction. This arises because the motor domain is separated from the backbone whereas the head-tail junction is connected to it. Still nearer the bare zone, essentially only the head-tail junction is included in slice 5. This results in peaks of density just outside the cylindrical backbone giving the filament a square appearance, as in the reconstruction. Slices 4 to 7 show a prominent density persisting in the same azimuthal position. This occurs at levels where D3 (the head-tail junction) and the link (the ELC domain of the B-wards head) are sectioned. In slices 6 and 7 the Z-wards head is sectioned through its motor domain giving rise to the spur. In slice 1 this head is sectioned through the interface between its motor and ELC domains corresponding to the axial part of the J-shaped feature. This gives rise to a peak of density separated from the link by a region of lower density.

Surface views of this best RJ model after filtering to low resolution are shown in Figure 1(d)-(f) where they may be compared with the reconstruction (Figure 1(a)-(c)). In Figure 1(f) the helical tracks of myosin heads appear zigzagged. Although the ridge contains only one motor domain, the model resembles the reconstruction, including the appearance of a spur along the link.



**Figure 6.** Atomic representation of the refined RJ model (run d). One of the four helical tracks is displayed in side-view. The secondary structure has been displayed as a ribbon diagram. The heavy chains and RLCs of the B-wards heads are shown mid-blue and red and those of the Z-wards heads in pale-blue and pink. The ELCs are shown yellow. The bare zone is at the top. Inset: The same model at lower magnification and with solid rendering and depth cueing. Molecules in successive crowns are in red, yellow and blue. The scale bar represents 145 Å.

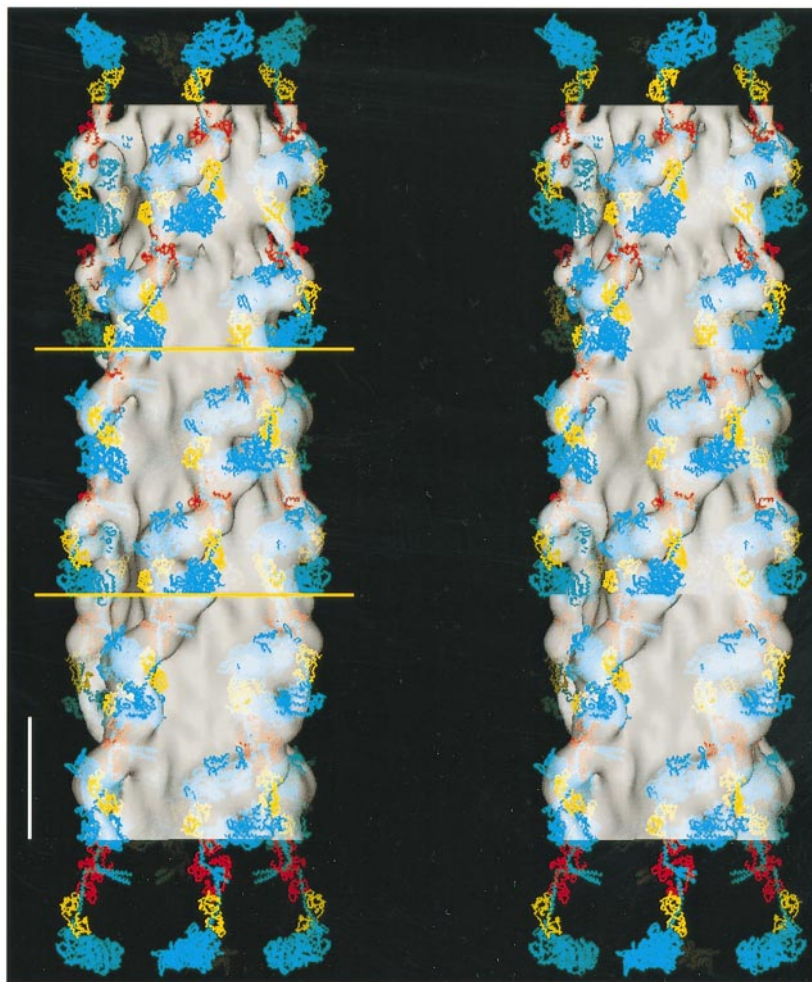


**Figure 7.** Comparison in stereo of the reconstruction and the refined RJ model (run d). The surfaces of three contour levels of the reconstruction are shown: top, contour level 135; middle, contour level 100; bottom, contour level 70. The division between these three sections is marked by horizontal lines. The surfaces of the reconstruction are semi-transparent so that the model inside the surfaces can be seen. The two heavy chains of each myosin molecule are shown light blue, the ELC yellow and the RLC red. At the two ends myosin molecules are shown without their neighbouring molecules. The scale bar represents 145 Å.

In Figure 1(e) this spur has enlarged to form the J-shaped feature. Thus the RJ model simulates rather closely the reconstruction including the J-shaped feature.

### RR models

With the head-tail junction located on the mid-point of the link, the arrangement of domains in the B-wards and Z-wards heads is very similar to that in the model of Padrón *et al.* (1998) built from S1 molecules and we therefore used this as our starting point. In the Padrón *et al.* (1998) model two anti-parallel overlapping S1s from neighbouring molecules are axially staggered but in close contact. Each ridge contains two motor domains and two ELC domains. Each link is formed from the two RLC domains of one myosin molecule but these are not in close proximity; the C $^{\alpha}$  atoms of the invariant proline residues are 30 Å apart (compared with 6 Å in our model of the regulated myosin with a compact head-tail junction) and the C-terminal  $\alpha$ -helices diverge rather than converge.

A filament model was built using an interacting dimer of S1s from the model of Padrón *et al.* (1998) and using the known helical symmetry of the filament. The cross-correlation coefficient of this S1

filament model with respect to the reconstruction (assuming a 100 Å radius backbone) was 0.876, substantially lower than for the refined RJ model described above. However, the Padrón *et al.* (1998) model was obtained by fitting by eye the S1 molecules within contour level 100 of the reconstruction and was not refined against the reconstruction on a voxel-by-voxel basis. We needed to determine whether such refinement would improve the match to the reconstruction.

To build a filament with rigid S1 molecules, ten parameters need to be specified. Three parameters are required to define the orientation of each of these two heads. Another three are required to define the spatial separation of the two heads. Finally the radius needs to be defined. The parameters of the original Padrón *et al.* (1998) model are given in Table 4. This parameterised model was refined against the reconstruction by the downhill simplex method, allowing the backbone radius also to vary but keeping the occupancy of the Z-wards S1 fixed at 1.0. On refinement the model altered dramatically such that the B-wards S1 moved radially inwards to lie almost wholly within the backbone (Table 4) and the model was no longer of the Padrón *et al.* (1998) type. Evidently if each S1 is rigid, a better match of the reconstruct-

**Table 4.** Parameters of model of Padrón *et al.* (1998) built from subfragment-1 molecules before and after refinement

	Cross-correlation coefficient	Radius <sup>a</sup> (Å)	Displacement of origins (Å) <sup>b</sup>			Backbone radius (Å)	Rotation of heads			Radius of heads (Å)		Centre of mass	
			$\Delta x$	$\Delta y$	$\Delta z$		x-axis	y-axis	z-axis	Inner	Outer		
Original model	0.876	101.2	-4.9	-14.4	-2.7	100.0	B	-27.7°	8.6°	15.3°	66.5	133.8	93.3
After downhill simplex refinement	0.920	107.2	-2.7	-11.9	-10.6	101.8	Z	182.6°	-44.4°	125.3°	78.1	148.5	112.1
							B	-20.4°	-3.7°	13.4°	54.3	122.9	85.7
							Z	188.9°	-52.8°	128.9°	90.8	156.5	120.8

The occupancy of both B-wards and Z-wards heads was fixed at 1.

<sup>a</sup> The radius of the midpoint between the origins of the two heads

<sup>b</sup>  $\Delta x$ ,  $\Delta y$  and  $\Delta z$  are the Cartesian components of the vector from this midpoint to the origin of one of the heads.

The origins of the two heads of one myosin molecule were chosen to lie at the invariant proline residue commencing the coiled coil.

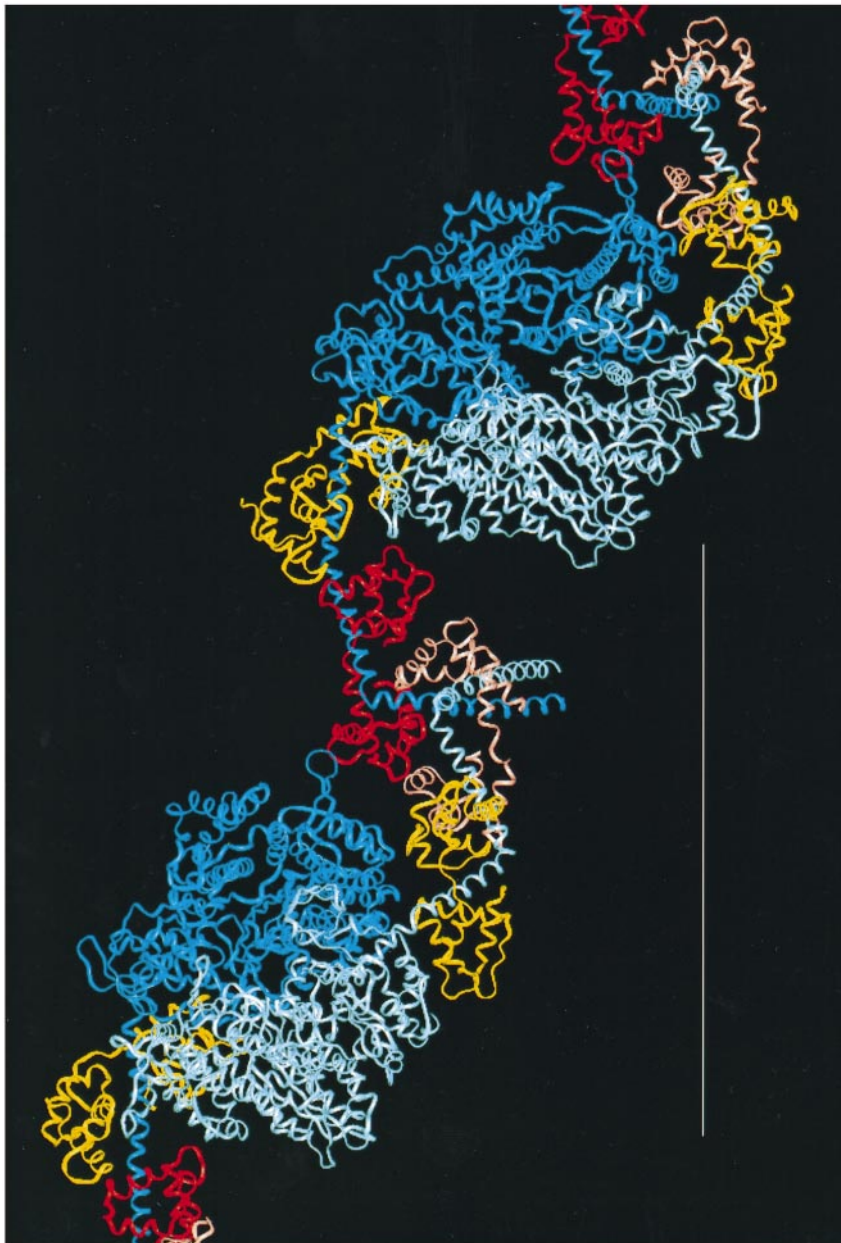


**Figure 8.** Atomic representation of the refined RR model (run f). One of the four helical tracks is displayed in side-view. The secondary structure has been displayed as a ribbon diagram. The heavy chains and RLCs of the B-wards heads are shown mid-blue and red and those of the Z-wards heads pale-blue and pink. ELCs are shown yellow. The bare zone is at the top. The scale bar represents 145 Å.

tion can be obtained by one head moving to such a low radius that it contributes little to the scoring. This is additional evidence that the ridge is formed from only one head.

In view of this deficiency of modelling with S1, it is important to know whether a better fit to the reconstruction could be obtained if the RLC domains of the heads were assembled into a head-tail junction, and the heads could tilt, flex and twist. We therefore built a model with our two-headed regulated myosin molecule adjusting the parameters by trial and error so that the atomic positions of the motor domains approximately fitted those of the S1s in the original Padrón *et al.* (1998) model. Using simulated annealing we then improved this model so that the atomic positions of the motor domains fitted as closely as possible to those in the original Padrón *et al.* (1998) model; the parameters of this RR model are given in Table 3. The rms deviation of atoms in the motor domains of one crown between this model and the original Padrón *et al.* (1998) model was only 3.5 Å. Correspondingly, the correlation coefficient of this model against the reconstruction (0.878) was similar to that of the original Padrón *et al.* (1998) model. Evidently forming a compact head-tail junction from the bases of the two heads of one molecule does not impair the fit to the reconstruction. As with the original Padrón *et al.* (1998) model, each ridge was made of two motor domains plus two ELC domains but now the link was formed from a compact head-tail junction.

On refinement of this RR model by the downhill simplex method allowing the weighting of the Z-wards head to vary, the cross-correlation coefficient rose from 0.878 to 0.930 (run f in Table 3). The model remained broadly of the Padrón *et al.* (1998) type with the B-wards and Z-wards motor domains of neighbouring molecules remaining in contact (Figure 8). In the original Padrón *et al.* (1998) model the B-wards head had an inner radius of only 66.5 Å (Table 4), substantially less than the radius of the backbone. However, on downhill simplex refinement of the RR model, the inner radius of the B-wards head moved to a higher and more acceptable value (86.0 Å) (Table 3). In the refined model there was some steric clash between the motor domains of neighbouring molecules but this was minimal considering the scoring was based solely on fit to the reconstruction rather than on steric packing. In side view the interacting motor domains did not completely fit within the ridge defined by contour level 100; their combined axial extent was greater by ~20 Å. Consistent with this, during refinement the occupancy of the Z-wards head decreased substantially from 1.0 to 0.30 suggesting that the Z-wards head spent only a fraction of its time in the ridge (R) position.

The appearance of transverse slices of the original Padrón *et al.* (1998) model and the refined RR model after filtering to low resolution is shown in Figure 3(d) and (e) respectively. The original Padrón *et al.* (1998) model gives blades which are

not sufficiently slewed and straight rather than curved. However, after downhill simplex refinement, the RR model gave a better match to the slew and curvature of the blades. However, not surprisingly, since the Padrón *et al.* (1998) model was formulated to fit only the zigzag of the helical tracks, the J-shaped feature is absent (Figure 3(d) and (e) slices 6 and 7).

By contrast, when the RR model was refined by simulated annealing, very substantial changes occurred so that the model was no longer of the Padrón *et al.* (1998) type. In three simulated annealing runs (not shown in Table 3), the Z-wards head moved away from the B-wards head towards a position (the J-position) approximately following the J-shaped feature in the reconstruction. The refined models resembled the RJ models and had similar cross-correlation coefficients (0.935, 0.946 and 0.950) and similar occupancies of the Z-wards head (0.42, 0.47 and 0.37). Evidently a better match to the reconstruction can occur if the Z-wards head moves to the J-position even though it is then absent from the ridge. We conclude that the RR model gives a less good fit to the reconstruction than the RJ model.

#### A variant of the RJ model: the RRJ model

In the refined RJ model discussed above, the Z-wards head is mobile and adopts the J position only for a fraction of the time. This raises the question of where this head is when it is not in the J position. One possibility is that it intermittently occupies the ridge position as well as the J position. Such a structure could be considered as a hybrid between the RJ and RR models and we therefore call it an RRJ model. To create an RRJ model we modified the RR model (refined by the downhill simplex method) so that the ELC and motor domains of the Z-wards head were also present in a second (J) position. This second position was determined by a further set of five parameters (defining bending at the three sites, tilting and torsional twisting). Initial values of these were determined by trial and error using the contour plots. We allowed all the other parameters defining the position of the B-wards head and the two positions of the Z-wards head, and the backbone radius to vary. The occupancies of the Z-wards head at the two positions were allowed to vary independently.

In all four simulated annealing runs (runs g-j in Table 3), the tip of the Z-wards head initially in the R position moved ~20 Å towards the Z-disc, increasing the separation between this head and the B-wards head to such an extent that it no longer lay inside the high density (>130) region of the ridge but in the shallow density on the Z-wards side of the ridge. Correspondingly, this movement reduced the separation between the two positions (R and J) of the Z-wards head. In one of the runs (run g) the Z-wards head in the J-position moved in the opposite direction resulting in the two positions of the Z-wards head substantially overlap-

ping. The occupancy of the Z-wards head in both positions was low ( $\sim 0.3$ ) consistent with the low density gradient on the Z-wards side of the ridge. Thus, although before refinement the two positions of the Z-wards head were very distinct, after annealing they were less separate and even overlapped. There was therefore no reason to consider the "ridge head" after refinement as belonging to the ridge, rather than the J position. Thus the refined RRJ models can be viewed as variants of the RJ model in which the Z-wards head adopts a range of angles rather than a fixed angle. In transverse sections these models gave a good match to the transverse sections (Figure 3(c)). However, despite the increased number of parameters used to construct them, the cross-correlation coefficient of these refined RRJ models was  $\sim 0.95$ , no higher than those of the refined RJ models.

## Discussion

We have succeeded in building a model of the relaxed tarantula myosin filament that gives a good fit to the three-dimensional reconstruction. The building block for this filament was a model of a two-headed regulated myosin molecule in which the RLCs of the two heads are closely apposed and, with their associated heavy chains, form a compact head-tail junction. This provides a structural basis to explain the intramolecular head-head interactions that underlie regulation and cooperativity in the molecule (Offer & Knight, 1996) and is consistent with information about the proximity of RLCs in myosin in intact muscle (Szent-Györgyi & Chantler, 1994). It is therefore important that we have been able to explain the structural features of the filament while retaining these interactions.

To fit our model of the regulated myosin molecule to the reconstruction, we allowed bending, tilting and twisting of the myosin heads and the number of possible structures was very large. Fortunately because we were modelling a three-dimensional reconstruction rather than an X-ray pattern, many structures could be eliminated by visual inspection. By comparing the relative spacings of the myosin domains to the features in the reconstruction, we were able to restrict the choice of models to only two main classes, the RJ and the RR. The RJ model gave a good match to the reconstruction both objectively, as measured by the cross-correlation coefficient, and subjectively explaining the main features of the reconstruction including the J-shape. It differs substantially from earlier models and has five principal novel features. First, the ridge of the reconstruction contains only one motor domain whereas all previous models had assumed that the ridge contained two motor domains. Second, the RLC domains of the two heads of one myosin molecule form a compact head-tail junction which is assigned to a prominent feature of the reconstruction, namely D3. Third, the

start of the coiled-coil tail is identified for the first time as the spoke, the connection between D3 and the backbone seen in the reconstruction. The fourth novel feature is that the Z-wards head is considered to be dynamic occupying the J-position only intermittently. Fifth, intermolecular interactions do not occur between motor domains as in previous models but exclusively between motor domains and light chains. In contrast, the RR model although explaining the zigzag nature of the helical tracks, did not account for the J-shaped feature and gave a lower cross-correlation coefficient.

In refining the models against the reconstruction we have used the entire density distribution in the cross-bridge annulus. We consider that a voxel-by-voxel comparison is preferable to fitting molecules within a contour boundary. In contour fitting, too much emphasis is likely to be placed on positioning the molecules within a contour boundary at the expense of trying to fit the peaks of density, which are likely to be the most reliable features of the reconstruction. The positions of these peak densities reflects the molecular boundary but is likely to be less influenced by neighbouring structures. The voxel-by-voxel comparison is particularly useful in the present case where the occupancy of the Z-wards head in the J-position is significantly less than 1.

The reconstruction of the negatively stained filaments we have used to fit our models has a resolution of about 50 Å (Crowther *et al.*, 1985). In negatively stained filaments the stain may penetrate some features of the structure more than others. Some collapse of the filament on drying is also inevitable yet the reconstruction assumes the structure is perfectly helical. Furthermore, although we have allowed flexibility at three sites along the head, in the real myosin molecule there may be further sites of flexibility. Finally, the conformations of the motor, ELC and RLC domains may be subtly different in the relaxed state from the ones in our model of the regulated myosin molecule, which came from the regulatory domain in the switched-on state. Hence, too much reliance on the finer details of the models should not be made.

Although our RJ model gave a good fit to the reconstruction, a definitive decision on its merits (and those of the alternative models) must await higher resolution micrographs, preferably those from cryo electron microscopy where artefacts from drying and staining are avoided. Alternatively, these models might be critically tested by comparing their Fourier transforms with the X-ray diffraction pattern of relaxed tarantula and Limulus muscle (Wray *et al.*, 1975; Wray, 1982). Wray *et al.* (1975) concluded from an analysis of the X-ray pattern of relaxed Limulus muscle that the principal diffracting unit was elongated and tilted  $\sim 30^\circ$  from the normal to the filament axis and slewed  $\sim 60^\circ$ . The principal diffracting structure is the ridge, especially D1 and D2 which are denser than D3. In our RJ model this part of the ridge has a tilt of  $\sim 65^\circ$  and a slew of  $\sim 60^\circ$ , similar to those

deduced by Wray *et al.* (1975). Following the reasoning of Wray *et al.* (1975), this model would therefore be expected broadly to account for the relative strengths of the layer lines in the X-ray diffraction patterns.

### Dynamic state of Z-wards head

The J-shaped feature has a lower density than the ridge. The weakness of the J-feature might result if the Z-wards head is not static but spends only about a fraction (about one-third) of its time in the J-position and the remainder of its time elsewhere. By way of alternative the motor domain might have a high temperature factor and swing through a range of angles about the J-position. Instead, the low density of this feature might arise because negative stain penetrates the Z-wards head more than the B-wards head; however, since the two heads are biochemically identical and lie at similar radii, we think this unlikely.

Support for the notion that myosin heads can flip between an ordered and a disordered conformation in the relaxed state is provided by studies of the effect of temperature on mammalian muscle (Wray 1987; Xu *et al.*, 1999). At high temperature relaxed rabbit muscle gives an X-ray diffraction pattern with strong layer lines, but as the temperature is lowered the layer lines become progressively weaker. Comparison between the temperature-dependence of the  $M.ATP = M.ADP.Pi$  equilibrium and of the degree of order has shown that the heads need to be in the  $M.ADP.Pi$  state to be helically ordered. It was concluded that the filaments are dynamic and at any instant of time those heads that happen to be in the  $M.ATP$  state are disordered while those in the  $M.ADP.Pi$  state are ordered.

### Intermolecular interaction between heads

In our RJ model there are intermolecular interactions between the motor domains of each myosin molecule and the light chains of its neighbours. These co-exist with the intramolecular RLC-RLC interactions implicit in the myosin model we used as a building block. The scallop myosin molecule itself shows not only regulatory properties but substantial cooperativity (Kalabokis & Szent-Györgyi, 1997) and, as discussed above, the intramolecular head-head interactions are thought to underlie this. However, in the filament this cooperativity is enhanced (Chantler *et al.* 1981) presumably mediated through the intermolecular contacts. It is intriguing that in our RJ model the contacts are between the tip of each motor domain and the RLC and ELC light chains of its neighbour since  $Ca^{2+}$  binds to the ELC close to its interface with RLC (Xie *et al.*, 1994). Such binding might thus exert a rather direct action on the motor domain of the neighbouring myosin molecule in contact with the ELC. Such intermolecular interactions might

contribute to regulation by inhibiting the heads from interacting with actin not only by locking them down on the surface but also by sterically blocking access of actin to the actin-binding sites.

### Proximity of active sites

Cross-linking studies on the related *Limulus* filaments with the bifunctional substrate  $bis_{22}ATP$  suggested that the active sites of neighbouring heads are close (Levine *et al.*, 1988). When filaments in the rigor state were treated with  $bis_{22}ATP$  in the presence of vanadate, they resumed the ordered appearance of the relaxed state. Such filaments were resistant to depolymerisation in high salt concentrations where the tails of the molecules would dissociate from one another, suggesting that  $bis_{22}ATP$  is able to cross-link the heads of neighbouring myosin molecules. In unpublished modelling studies of the conformational flexibility of  $bis_{22}ATP$  when it cross-links two anti-parallel S1 molecules, we have found that for  $bis_{22}ATP$  to bind to both active sites, the distance between the Trp131 residues at the mouths of the two active sites and the distance between the Ser324 residues should total between 27-39 Å.

In the original Padron *et al.* (1998) model this criterion for the active sites to be sufficiently close for cross-linking is met, since the Trp-Trp distance is 8.8 Å and the Ser-Ser distance is 20.6 Å. It is also met in the two-headed approximation to the Padrón *et al.* (1998) model (Trp-Trp distance 12.8 Å and Ser-Ser distance 22.5 Å). After downhill simplex refinement of this model, the criterion is nearly met (Trp-Trp distance 20.7 Å and Ser-Ser distance 23.1 Å). In contrast, in the RJ model the active sites are much further apart (Trp-Trp distance 39.1 Å and Ser-Ser distance 32.4 Å) and  $bis_{22}ATP$  could not cross-link the heads in these positions. However, in this model the Z-wards heads spend the majority of their time in a disordered state and it is possible that cross-linking could occur at times when the heads are close enough. Hence our RJ model is not inconsistent with the cross-linking experiments. It is not known what fraction of the heads were cross-linked in the experiments of Levine *et al.* (1988). Nor is it known whether, as a result of cross-linking, the structure is perturbed from the native since a reconstruction from the cross-linked material is not available nor has this been examined by X-ray fibre diffraction. It is quite conceivable that the cross-linking of a few cross-bridges is sufficient to stabilise the filament and these cross-bridges have a different arrangement from the one present in the native relaxed filament.

### Orientation of coiled-coil tail

The myosin tails in the backbone of invertebrate muscle thick filaments, like those of vertebrate filaments (Chew & Squire, 1995), are thought to be

tilted at only a small angle to the filament axis (Wray, 1979). The appearance of longitudinal striations in the backbone of negatively stained tarantula thick filaments (Crowther *et al.*, 1985) also suggests that the majority of the tail is nearly axial. However a near-perpendicular orientation at the start of the coiled-coil tail is implicit in the models of Levine *et al.* (1988) and of Padrón *et al.* (1998) if the heads join onto a fully formed coiled coil. In our models too the tilt was near  $90^\circ$ . This carries no implication about the orientation of the rest of the coiled coil and indeed we suppose that the coiled-coil tail bends either before or when it meets the backbone to become nearly axial. The radius of the invariant proline residues commencing the coiled coil in the best RJ model is  $\sim 113 \text{ \AA}$ . The tilt and slew of this model imply that the coiled coil, if straight, would reach the surface of the backbone (assumed to have a radius of  $90 \text{ \AA}$ ) after only a distance of  $\sim 27 \text{ \AA}$  or  $\sim 18$  residues so our model is compatible with a high fraction ( $\sim 98\%$ ) of the coiled coil being nearly axial.

### Structure of thick filaments from other species

Although our models were devised to fit the reconstruction of tarantula filaments, similar filament architectures would be expected to be present in the muscles of scorpion or Limulus which are also chelicerate arthropods. Despite their similarity, Kensler *et al.* (1985) showed that the radius ( $134 \text{ \AA}$ ) of the centre of mass of the heads in tarantula was larger than that in scorpion ( $114\text{--}128 \text{ \AA}$ ) but smaller than that in Limulus filaments ( $155 \text{ \AA}$ ). This is hard to explain by models in which only the motor domains participate in intermolecular interactions between myosin molecules, since the sequence of the motor domain tends to be highly conserved. However, in our RJ model where neighbouring myosin molecules along a helical track form motor-RLC contacts, the size of the RLC might determine the radius of the heads. Although the molecular weight of scorpion RLC is not known, it is noteworthy that the molecular weight of one of the Limulus RLC's ( $31 \text{ kDa}$ , Sellers 1981) is higher than that of tarantula RLC ( $26 \text{ kDa}$ , Craig *et al.*, 1987).

Myosin filaments from different species have similar surface lattices and they are likely therefore to be constructed on similar principles (Squire, 1971, 1986). On the basis of their X-ray diffraction patterns Wray *et al.* (1975) suggested that the arrangement of myosin heads on the surface of the filaments from frog (and by implication other vertebrates) resembled those from the Limulus group. Models of frog filaments can be constructed with helical tracks of interlocking S-shaped myosin molecules analogous to our tarantula RJ model and it is possible that similar interactions occur widely in the construction of myosin filaments. It remains to be seen whether this is so and whether the myosin filaments of bony fish are unique in having parallel rather than splayed heads (Hudson *et al.*, 1997).

## Methods

### Reconstruction data

The three-dimensional map of protein density distribution in negatively stained tarantula filaments was that provided by the helical reconstruction of Crowther *et al.* (1985). The data used for that reconstruction included in an axial direction layer lines up to and including the ninth (corresponding to  $1/48 \text{ \AA}^{-1}$ ) and out to  $1/37 \text{ \AA}^{-1}$  in a radial direction on the strong first layer line. The protein density distribution of the reconstruction was reformatted into a set of 20 binary files, each file corresponding to a serial transverse slice  $7.25 \text{ \AA}$  thick and containing  $93 \times 93$  pixels of side  $4.2 \text{ \AA}$ ; the set thus defined a segment  $145 \text{ \AA}$  long of the filament containing all the information for the morphological unit. It was assumed that there was no differential shrinkage in the radial direction. Densities of the map were floated to a region of high radius in the background (with densities of about 10 on this new scale). For viewing a set of contours of the reconstruction in Insight II or O, the same data was reformatted to produce a grid file (Insight II) or an Xplor-style map file (O). With regard to the information content of the reconstruction, there were ten plots of amplitude against reciprocal radius and correspondingly ten plots of phase versus reciprocal radius. We can imagine sampling of the layer lines at intervals of the reciprocal of the thick filament diameter (i.e.  $1/320 \text{ \AA}^{-1}$ ). For a resolution of  $50 \text{ \AA}$  this would give seven sampling positions per layer line or a total of 140 possible observations. The number of these sampling positions where the plot was significantly above the local noise was 56. Since the number of parameters we used in the modelling was only 16, the model was over-determined by the experimental data.

### Transverse slices of model and scoring

The models of tarantula thick filaments were created with the molecular graphics application Insight II version 95 (Biosym/MSI, San Diego, CA). To minimise computation, a filament only three crowns long was made, the head-tail junctions of the second crown being placed at the origin of the filament axis. The output pdb file of the atomic coordinates of the filament was edited to include atoms only within a central segment  $160 \text{ \AA}$  long.

To compare quantitatively a model with the reconstruction, each  $C^\alpha$  atom of the filament model was represented by a sphere of  $3 \text{ \AA}$  radius. The volume contribution these spheres made to each pixel in a  $93 \times 93 \times 20$  array ( $145 \text{ \AA}$  long) was calculated. The backbone of the filament was represented by a cylinder and the volume contribution this made to each pixel was included. The contributions from the heads and the backbone were scaled to be equal (since the molecular weight of the two heads of a myosin molecule is approximately equal to that of the tail). When it was desired to reduce the weighting of the ELC domain and motor domain of one of the heads, the contributions from atoms in these domains were correspondingly reduced. The resulting pixel densities were scaled to lie in the range 0 to 255. The binary files produced were imported into SPIDER (Frank *et al.*, 1981). The slices were stacked (with appropriate rotation for successive morphological units) to produce a volume  $5 \times 145 \text{ \AA}$  long. After interpolation to a volume  $93 \times 93 \times 175$  pixels (so that the pixels were approximately cubic), such volumes were low-pass filtered using a Gaussian func-

tion to a resolution of 50 Å to blur the models appropriately for comparison with the reconstruction without introducing ripples. The central  $3 \times 145$  Å segment was selected giving a volume  $93 \times 93 \times 105$  pixels to be compared with a similar volume from the reconstruction. Rotational alignment of these volumes was obtained by comparison of projections of these volumes down the filament axis. After appropriate rotation of the model volume, the translational alignment of these volumes was obtained by comparison of side-on projections of these volumes. Each model was scored by the cross-correlation coefficient obtained from the aligned volumes. A mask function restricted the comparison to an annulus bounded by radii 80 and 195 Å.

### Refining the filament model

The models were refined against the reconstruction by the downhill simplex method of Nelder & Mead (1965). Because the construction and scoring of each filament model required the use both of Insight II and SPIDER, the downhill simplex program of Press *et al.* (1992) was rewritten as a shell script directing the shell script that created each filament model, six C programs which produced the reflection, extension, contraction or shrinkage points of the simplex, a C program which created the image files and a SPIDER program which aligned and scored the model against the reconstruction.

The downhill simplex method alone finds a local fit close to the starting structure. We therefore used the method of simulated annealing described by Press *et al.* (1992), based on the downhill simplex method, to explore conformational space more globally. To determine whether a move of the simplex to a new position should be made, the cross-correlation coefficients for all the vertices of the current simplex were temporarily diminished, while those for the reflection, extension or contraction points augmented, by an amount  $T \ln x$  where  $x$  is a random number between 0 and 1, and  $T$  (analogous to temperature) initially 0.02 was allowed to decrease linearly to zero during the simulation in steps of 0.002. 100 iterations were performed at each temperature.

A total of 16 parameters were varied for the case when each head adopted only one position. These are the radius, tilt, slew and rotation of each myosin molecule together with six parameters defining the (independent) bending of the two heads at the three sites, two parameters defining the tilt of the two heads with respect to the tail and two defining the torsional twist. In addition the weighting of the ELC domain and motor domain of the second head and the backbone radius were treated as variables. For the models where the Z-wards head adopted two positions, 21 parameters were required.

### Acknowledgements

We thank Drs R. Craig, R. Kensler, R. Levine, E. Morris, J. Squire and J. Wray for discussion. R.P. and L.A. dedicate this paper to the memory of Dr Humberto Fernández-Morán and to Dr Leonardo Mateu on the occasion of his 60th birthday. This work was supported by a grant from CONICIT. The research of R.P. was supported in part by an International Research Scholars grant from the Howard Hughes Medical Institute.

### References

- Burgess, S. A., Walker, M. L., White, H. D. & Trinick, J. (1997). Flexibility within myosin heads revealed by negative stain and single-particle analysis. *J. Cell Biol.* **139**, 675-681.
- Chantler, P. D., Sellers, J. R. & Szent-Györgyi, A. G. (1981). Cooperativity in scallop myosin. *Biochemistry*, **20**, 210-216.
- Chew, M. K. W. & Squire, J. M. (1995). Packing of  $\alpha$ -helical coiled-coil myosin rods in vertebrate muscle thick filaments. *J. Struct. Biol.* **115**, 233-249.
- Craig, R. & Padrón, R. (1982). Structure of tarantula muscle thick filaments. *J. Muscle Res. Cell Motil.* **3**, 487.
- Craig, R., Padrón, R. & Kendrick-Jones, J. (1987). Structural changes accompanying phosphorylation of tarantula muscle thick filaments. *J. Cell Biol.* **105**, 1319-1327.
- Crowther, R. A., Padrón, R. & Craig, R. (1985). Arrangement of the heads of myosin in relaxed thick filaments from tarantula muscle. *J. Mol. Biol.* **184**, 429-439.
- Dominguez, R., Freyzon, Y., Trybus, K. M. & Cohen, C. (1998). Crystal structure of a vertebrate smooth muscle myosin motor domain and its complex with the essential light chain: visualisation of the pre-power stroke. *Cell*, **94**, 559-571.
- Elliott, A. & Offer, G. (1978). Shape and flexibility of the myosin molecule. *J. Mol. Biol.* **123**, 505-519.
- Fisher, A. J., Smith, C. A., Thoden, J. B., Smith, R., Sutoh, K., Holden, H. & Rayment, I. (1995). X-ray structures of the myosin motor domain of dictyostelium discoideum complexed with  $MgADP \cdot BeF_x$  and  $MgADP \cdot AlF_4$ . *Biochemistry*, **34**, 8960-8972.
- Frank, J., Shimkin, B. & Dowse, H. (1981). SPIDER: a modular software system for electron image processing. *Ultramicroscopy*, **6**, 343-358.
- Houdusse, A. & Cohen, C. (1996). Structure of the regulatory domain of scallop myosin at 2 Å resolution: implications for regulation. *Structure*, **4**, 21-32.
- Hudson, L., Harford, J. J., Denny, R. C. & Squire, J. M. (1997). Myosin head configuration in relaxed fish muscle: resting state myosin heads must swing axially by up to 150 Å or turn upside down to reach rigor. *J. Mol. Biol.* **273**, 440-455.
- Kalabokis, V. N. & Szent-Györgyi, A. G. (1997). Cooperativity and regulation of scallop myosin and myosin fragments. *Biochemistry*, **36**, 15834-15840.
- Kensler, R. W. & Levine, R. J. C. (1982). An electron microscopic and optical diffraction analysis of the structure of Limulus telson muscle thick filaments. *J. Cell Biol.* **92**, 443-451.
- Kensler, R. W., Levine, R. J. C. & Stewart, M. (1985). Electron microscopic and optical diffraction analysis of the structure of scorpion muscle thick filaments. *J. Cell Biol.* **101**, 395-401.
- Levine, R. J. C., Kensler, R. W., Reedy, M. C., Hofmann, W. & King, H. A. (1983). Structure and paramyosin content of tarantula thick filaments. *J. Cell Biol.* **97**, 186-195.
- Levine, R. J. C., Chantler, P. D. & Kensler, R. W. (1988). Arrangement of myosin heads on Limulus thick filaments. *J. Cell Biol.* **107**, 1739-1747.
- Levine, R. J. C., Chantler, P. D., Kensler, R. W. & Woodhead, J. (1991). Effects of phosphorylation by myosin light chain kinase on the structure of Limulus thick filaments. *J. Cell Biol.* **113**, 563-572.

- Mendelson, R. A., Morales, M. F. & Botts, J. (1973). Segmental flexibility of the S-1 moiety of myosin. *Biochemistry*, **12**, 2250-2255.
- Mendelson, R. A., Schneider, D. K. & Stone, D. B. (1996). Conformations of myosin subfragment 1 ATPase intermediates from neutron and X-ray scattering. *J. Mol. Biol.* **256**, 1-7.
- Nelder, J. A. & Mead, R. (1965). The simplex method for function minimisation. *Computer J.* **7**, 308-313.
- Offer, G. & Knight, P. (1996). The structure of the head-tail junction of the myosin molecule. *J. Mol. Biol.* **256**, 407-416.
- Padrón, R., Pante, N., Sosa, H. & Kendrick-Jones, J. (1991). X-ray diffraction study of the structural changes accompanying phosphorylation of tarantula muscle. *J. Muscle Res. Cell Motil.* **12**, 235-241.
- Padrón, R., Guerrero, J. R., Alamo, L., Granados, M., Gherbesi, N. & Craig, R. (1993). Direct visualization of myosin filament symmetry in tarantula striated muscle by electron microscopy. *J. Struct. Biol.* **111**, 17-21.
- Padrón, R., Alamo, L., Guerrero, J. R., Granados, M., Uman, P. & Craig, R. (1995). Three-dimensional reconstruction of thick filaments from rapidly frozen, freeze-substituted tarantula muscle. *J. Struct. Biol.* **115**, 250-257.
- Padrón, R., Alamo, L., Murgich, J. & Craig, R. (1998). Towards an atomic model of the thick filaments of muscle. *J. Mol. Biol.* **275**, 35-41.
- Padrón, R., Alamo, L. & Craig, R. (1999). Three-dimensional reconstruction of frozen hydrated thick filaments from tarantula muscle. *Biophys. J.* **76**, A34.
- Press, W. H., Teukolsky, S. A., Vetterling, W. T. & Flannery, B. P. (1992). *Numerical Recipes in C*, Cambridge University Press, Cambridge.
- Rayment, I., Rypniewski, W. R., Schmidt-Base, K., Smith, R., Tomchick, D. R., Benning, M. M., Winkelmann, D. A., Wesenberg, G. & Holden, H. M. (1993). Three-dimensional structure of myosin subfragment-1: a molecular motor. *Science*, **261**, 50-58.
- Sellers, J. R. (1981). Phosphorylation-dependent regulation of Limulus myosin. *J. Biol. Chem.* **256**, 9274-9278.
- de Silva, A. G. (1998). X-ray diffraction studies of the conformation of myosin heads in relaxed frog muscle. PhD thesis, University of London.
- Slyter, H. S. & Lowey, S. (1967). Substructure of the myosin molecule as visualized by electron microscopy. *Proc. Natl Acad. Sci. USA*, **58**, 1611-1618.
- Squire, J. M. (1971). General model for the structure of all myosin-containing filaments. *Nature*, **233**, 457-462.
- Squire, J. M. (1986). Muscle myosin filaments: internal structure and crossbridge organization. *Comments Mol. Cell. Biophys.* **3**, 155-177.
- Stewart, M., Kensler, R. W. & Levine, R. J. C. (1981). Structure of Limulus telson muscle thick filaments. *J. Mol. Biol.* **153**, 781-790.
- Stewart, M., Kensler, R. W. & Levine, R. J. C. (1985). Three-dimensional reconstruction of thick filaments from Limulus and scorpion muscle. *J. Cell Biol.* **101**, 402-411.
- Sugimoto, Y., Tokunaga, M., Takezawa, Y., Ikebe, M. & Wakabayashi, K. (1995). Conformational changes of the myosin heads during hydrolysis of ATP as analyzed by X-ray solution scattering. *Biophys. J.* **68**, 29s-34s.
- Szent-Györgyi, A. G. & Chantler, P. D. (1994). Control of contraction by calcium binding to myosin. In *Myology* (Engel, A. G. & Franzini-Armstrong, C., eds), pp. 506-528, McGraw-Hill, New York.
- Vibert, P. & Craig, R. (1985). Structural changes that occur in scallop myosin filaments upon activation. *J. Cell Biol.* **101**, 830-837.
- Wakabayashi, K., Tokunaga, M., Kohno, I., Sugimoto, Y., Hamanaka, T., Takezawa, Y., Wakabayashi, T. & Amemiya, Y. (1992). Small-angle synchrotron X-ray scattering reveals distinct shape changes of the myosin head during hydrolysis of ATP. *Science*, **258**, 443-447.
- Whittaker, M., Wilson-Kubalek, E. M., Smith, J. E., Faust, L., Milligan, R. A. & Sweeney, L. (1995). A 35-Å movement of smooth muscle myosin on ADP release. *Nature*, **378**, 748-751.
- Wray, J. S. (1979). Structure of the backbone in myosin filaments of muscle. *Nature*, **277**, 37-40.
- Wray, J. S. (1982). Organisation of myosin in invertebrate thick filaments. In *Basic Biology of Muscles: A Comparative Approach* (Twarog, B., Levine, R. J. C. & Dewey, M. M., eds), pp. 29-36, Raven Press, New York.
- Wray, J. S. (1987). Structure of relaxed myosin filaments in relation to nucleotide state in vertebrate skeletal muscle. *J. Muscle Res. Cell Motil.* **8**, 62.
- Wray, J. S., Vibert, P. J. & Cohen, C. (1974). Cross-bridge arrangements in Limulus muscle. *J. Mol. Biol.* **88**, 343-348.
- Wray, J. S., Vibert, P. J. & Cohen, C. (1975). Diversity of cross-bridge configurations in invertebrate muscles. *Nature*, **257**, 561-564.
- Xie, X., Harrison, D. H., Schlichting, I., Sweet, R. M., Kalabokis, V. N., Szent-Györgyi, A. G. & Cohen, C. (1994). Structure of the regulatory domain of scallop myosin at 2.8 Å resolution. *Nature*, **368**, 306-312.
- Xu, S., Gu, J., Rhodes, T., Belknap, B., Rosenbaum, G., Offer, G., White, H. & Yu, L. C. (1999). The M.ADP.Pi state is required for helical order in the thick filaments of skeletal muscle. *Biophys. J.* **77**, 2665-2676.

Edited by M. F. Moody

(Received 16 June 1999; received in revised form 2 March 2000; accepted 6 March 2000)